



HAL
open science

DNA Hybridization Measured with Graphene Transistor Arrays

Kokoura Mensah, Ismaïl Cissé, Aurélie Pierret, Michael Rosticher, José Palomo, Pascal Morfin, Bernard Placais, Ulrich Bockelmann

► **To cite this version:**

Kokoura Mensah, Ismaïl Cissé, Aurélie Pierret, Michael Rosticher, José Palomo, et al.. DNA Hybridization Measured with Graphene Transistor Arrays. *Advanced Healthcare Materials*, 2020, 9 (16), pp.2000260. 10.1002/adhm.202000260 . hal-02989040

HAL Id: hal-02989040

<https://hal.science/hal-02989040v1>

Submitted on 12 Nov 2020

HAL is a multi-disciplinary open access archive for the deposit and dissemination of scientific research documents, whether they are published or not. The documents may come from teaching and research institutions in France or abroad, or from public or private research centers.

L'archive ouverte pluridisciplinaire **HAL**, est destinée au dépôt et à la diffusion de documents scientifiques de niveau recherche, publiés ou non, émanant des établissements d'enseignement et de recherche français ou étrangers, des laboratoires publics ou privés.

DNA Hybridization Measured with Graphene Transistor Arrays

Kokoura Mensah, Ismail Cissé, Aurélie Pierret, Michael Rosticher, José Palomo, Pascal Morfin, Bernard Plaçais, and Ulrich Bockelmann*

Arrays of field-effect transistors are fabricated from chemical vapor deposition grown graphene (GFETs) and label-free detection of DNA hybridization performed down to femtomolar concentrations. A process is developed for large-area graphene sheets, which includes a thin Al_2O_3 layer, protecting the graphene from contamination during photolithographic patterning and a SiO_x capping for biocompatibility. It enables fabrication of high-quality transistor arrays, exhibiting stable close-to-zero Dirac point voltages under ambient conditions. Passivation of the as-fabricated chip with a layer composed of two different oxides avoids direct electrochemical contact between the DNA solutions and the graphene layer during hybridization detection. DNA probe molecules are electrostatically immobilized via poly-L-lysine coating of the chip surface. Adsorption of this positively charged polymer induces a positive shift of the Dirac point and subsequent immobilization of negatively charged DNA probes induces a negative shift. Spatially resolved hybridization of DNA sequences is performed on the GFET arrays. End-point as well as real-time *in situ* measurements of hybridization are achieved. A detection limit of 10 fM is observed for hybridization of 20-nucleotide DNA targets. Typical voltage signals are around 100 mV and spurious drifts below 1 mV per hour.

In field-effect devices, such as the field-effect transistor (FET) or metal–insulator–semiconductor capacitors (MIS capacitor), the concentration of a layer of charge carriers is modulated by an external electric field.^[2] Biomolecule sensing can be achieved by the field effect. For instance, a DNA molecule immobilized on an electrolyte-gated FET surface in contact with an aqueous electrolyte solution, can be detected by the electric field associated with the intrinsic charge of the molecule. Field-effect sensing of biomolecules has been achieved with planar silicon devices,^[3–5] silicon nanowire FETs,^[6–11] carbon nanotubes,^[12,13] and graphene structures.^[14,15] Among these materials, graphene is particularly promising for biosensing applications,^[16–18] because it combines high room-temperature mobility of charge carriers, the possibility of a short (nanometer scale) distance between the graphene monolayer and the molecules to be detected, and the possibility of fabricating transistor arrays with surface areas of tens of square millimeters at moderate cost.^[19,20] Several methods to detect

1. Introduction


Controlling the electronic properties of a device using externally applied gate voltages was a milestone in modern electronics.^[1]

DNA hybridization rely on labeling of target molecules with fluorophores,^[21,22] nanoparticles,^[23] radioactive elements, or enzymes.^[24–26] Although these techniques are currently widely used they exhibit some inconveniences. The labeling step can be labor-intensive, time-consuming, expensive, and homogeneous labeling is not always achieved. Moreover, labels may sometimes reduce the specificity of sequence recognition by hybridization and may exhibit reproducibility issues, such as photobleaching of fluorophores and batch-to-batch variation in enzyme activity. Therefore, label-free detection of DNA by its intrinsic molecular charge attracts interest.

Some investigations of biomolecule detection with graphene structures have been published recently. Kwak et al.^[27] detected glucose with a FET fabricated from CVD-grown graphene. Measuring shifts in Dirac point and differential drain-source current, they detected glucose levels in a range of 3–11 mM. According to the authors, this sensitivity is adapted to diabetes diagnostics. Khatayevich et al.^[28] were able to detect protein with a FET fabricated from exfoliated graphene. Probe molecules were attached to the graphene via self-assembling multifunctional peptides. Chen et al.^[29] fabricated a FET structure from a

Dr. K. Mensah, Dr. I. Cissé, Dr. U. Bockelmann^[+]
Laboratoire Nanobiophysique
ESPCI Paris
Université PSL
CNRS
Paris 75005, France
E-mail: ulrich.bockelmann@inserm.fr

Dr. A. Pierret, Dr. M. Rosticher, J. Palomo, P. Morfin, Dr. B. Plaçais
Laboratoire de Physique de l'Ecole Normale Supérieure
ENS
Université PSL
CNRS
Sorbonne Université
Université Paris-Diderot
Paris 75005, France

 The ORCID identification number(s) for the author(s) of this article can be found under <https://doi.org/10.1002/adhm.202000260>

^[+]Present address: Institut Cochin, 22 rue Méchain, Paris 75014, France

DOI: 10.1002/adhm.202000260

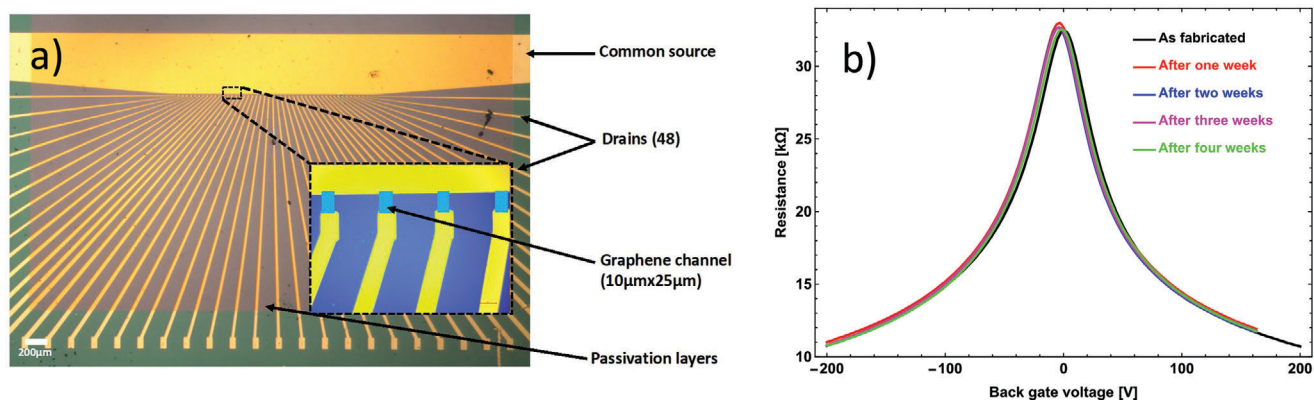


Figure 1. a) Microscopic image of a graphene FET array device. The graphene sheet is patterned by a lithography process into 48 individual channels. Each channel is connected to a common source and an individual drain electrode (Ti/Au). The chip is passivated with 40 nm Al_2O_3 (ALD) and 50 nm SiO_x (PECVD). The passivation layers are removed on the extremities of the electrodes to make electrical contact. b) Electrical source-drain resistance R_{DS} (kΩ) as a function of back gate voltage (V). A bipolar transfer curve is observed involving two types of charge carriers. The predominant carrier type can be tuned from holes (left) to electrons (right). The charge-neutrality point V_{cnp} corresponds to the maximum in R_{DS} . V_{cnp} is close to zero. The presented time series shows that this device characteristics is stable for more than a month. $U_{\text{DS}} = 0.5$ V.

graphene film prepared by CVD on copper foils and transferred onto a SiO_2 wafer. They reported hybridization of DNA oligonucleotides, down to target concentrations of 1 pM. Xu et al.^[30] fabricated small arrays, containing eight individual FETs, from CVD graphene and showed site-specific detection of target DNA. Biotinylated probe oligonucleotides were attached to graphene by adsorption of biotinylated BSA and incubation with streptavidin.

Here, we report on the use of graphene field-effect transistor (GFET) arrays for label-free detection of DNA with high specificity, high sensitivity, and low-drift. Specificity is obtained by hybridization under appropriate conditions of salt and temperature using short DNA probes complementary to the DNA target. High sensitivity stems from a good transducing capability of our GFET arrays, which result from two original points. On the one hand, we use an innovative process that strongly reduces degradation of graphene during device fabrication. On the other hand, we use a nanometer-thin protection layer, which separates graphene from the electrolyte solution during DNA hybridization and electronic measurement. Combined they avoid graphene contamination, which causes a voltage-shift of the Dirac point that is detrimental to charge carrier mobility and detection sensitivity. Moreover, our device exhibited very stable threshold voltages under different electronic configurations that allowed probe hybridization and target DNA detection. The combination of high sensitivity and low drift allowed real time detection of probe/target hybridization.

2. Results

2.1. Preparation and Initial Characterization of Graphene Field-Effect Transistor Arrays

We fabricated (see Experimental Section) arrays consisting of 48 linear-arranged graphene FETs, with each individual FET exhibiting a sensing area of $10 \mu\text{m} \times 25 \mu\text{m}$ each connected to a common source and an individual drain electrode (Figure 1a). First, elec-

trical characterization of the device was carried out in dry room-temperature environment, by measuring the drain current as a function of source-drain and back gate voltages (Figure 1b). In this configuration, a highly doped Si substrate covered by a 1 µm thick thermal SiO_2 oxide served as the back gate. The mobility of the device is in the range of $1000\text{--}4000 \text{ cm}^2 \text{ V}^{-1} \text{ s}^{-1}$.

In contrast to earlier work on biosensing with graphene, we decided to cover the graphene sensing layer with a thin insulator. The goal being to obtain graphene passivation for a good reproducibility in biomolecule detection when the device surface is immersed in aqueous solution (see Experimental Section). The chip is fixed on a ceramic package, wire bonded and a plastic well protects the electrical connections during subsequent incubations with aqueous solutions. This way, we avoid solution-induced doping of graphene and electrochemical effects that are difficult to control. To maintain high sensitivity of detection, the insulating layer exhibits a thickness of only a few tens of nanometers. The thin dielectric layer also reduces the risk that the required attachment of probe molecules degrades the intrinsically high carrier mobility of the graphene. Atomic layer deposition (ALD) was used for this gate insulator, to achieve negligible leakage current and good homogeneity of the threshold-voltages across the field-effect transistor array. For 40 nm of Al_2O_3 , our devices showed significant drift and the gate insulators were ablated during measurements under KCl electrolyte solution. When a 50 nm thick SiO_x coating was added by plasma enhanced chemical vapor deposition (PECVD), the device showed good stability and low drift, with high sensitivity biomolecule detection. In the final configuration, the SiO_x layer is the sensor surface and protects the buried Al_2O_3 layer from contact with the electrolyte (a schematic view is provided in Supporting Information).

2.2. Immobilization of DNA Probes and Detection of Biomolecule Adsorption

After thoroughly rinsing the chip with deionized water it was immersed in a poly(L-lysine) (PLL) polymer solution for 30 min,

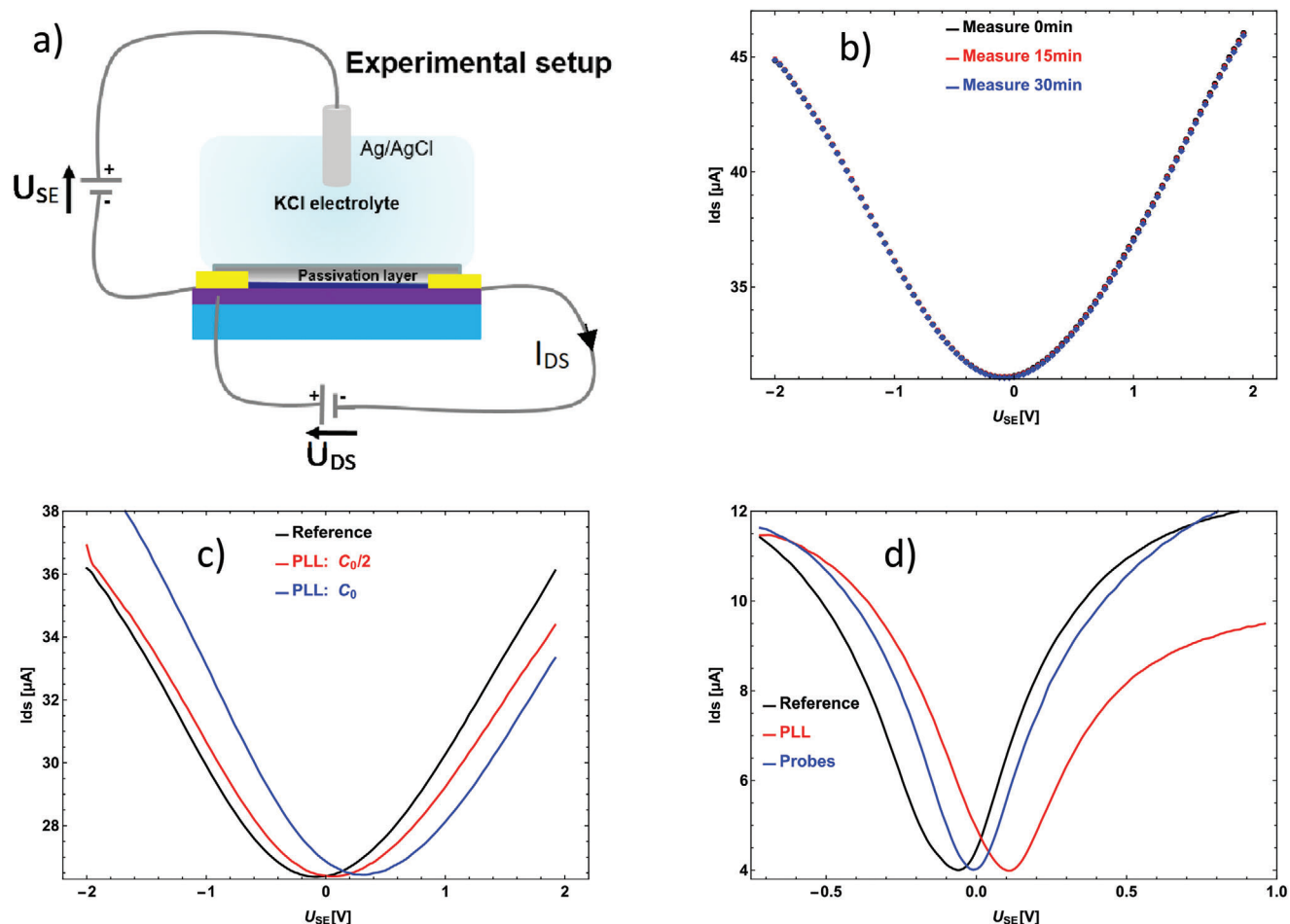


Figure 2. a) Schematic illustration of the configuration used for electronic detection of biomolecules. b) Absence of temporal drift on a time-scale of 30 min. $U_{DS} = 1$ V. c) Device response to PLL adsorption. $U_{DS} = 0.8$ V. d) Device response to PLL adsorption (red) and probe immobilization (blue). PLL adsorption induces a right shift of V_{cnp} and DNA probe immobilization a left shift. $U_{DS} = 10$ mV. In all measurements of this figure we used [KCl] = 25 mM.

air-dried and conserved overnight at room temperature. PLL is a positively charged polymer that readily adsorbs to the negatively charged silica surface of our device. In all the subsequently described electrical measurements of biomolecule adsorption or DNA hybridization, the back-gate is disconnected. Instead, a voltage U_{SE} is applied between a common source contact and an Ag/AgCl reference electrode immersed in a KCl solution covering the array. This way, the drain current I_{DS} of each FET is measured as a function of source-drain voltage U_{DS} and source-electrolyte voltage U_{SE} (Figure 2a). We observed that PLL adsorption induces positive gate-voltage shifts of the graphene Dirac point that increase with PLL concentration (Figure 2c). For the PLL adsorption protocol given in the Experimental Section, we measured a shift of the charge-neutrality-point gate voltage $\Delta V_{cnp} = +185 \pm 104$ mV.

DNA oligonucleotide probes (20-mer at 1 μM concentration) were immobilized onto the PLL coated surface. The probes were dissolved in PBS (see Experimental Section) and a 0.1 μL drop of the solution deposited, covering 8–10 individual FETs of the array. Adsorption of the DNA probe induces negative shifts of V_{cnp} . The shifts of DNA and PLL are of opposite sign,

as expected due to DNA and PLL having intrinsic molecular charges of opposite sign (Figure 2d). The charge of the immobilized molecules induces a shift in surface potential that, by field effect, is transduced to a shift in the charge neutrality point of the GFET. Immobilization of DNA probes does not fully compensate the positive charge of the PLL layer, which suggests that any remaining positive charge can induce non-specific adsorption of DNA targets during the hybridization process. Indeed, efficient blocking is required for DNA detection in the microarray format. Following earlier work,^[3] we combined a chemical and physical blocking procedure: the chip is first incubated in acetic anhydride and subsequently in a solution containing 21-mer oligonucleotides (Lprime). Lprime sequence differs in sequence to other molecules under study to avoid cross-hybridization.

2.3. Electronic Detection of DNA Hybridization

Molecular recognition occurs at the surface of the gate insulator, with short probe DNA oligonucleotides electrostatically attached

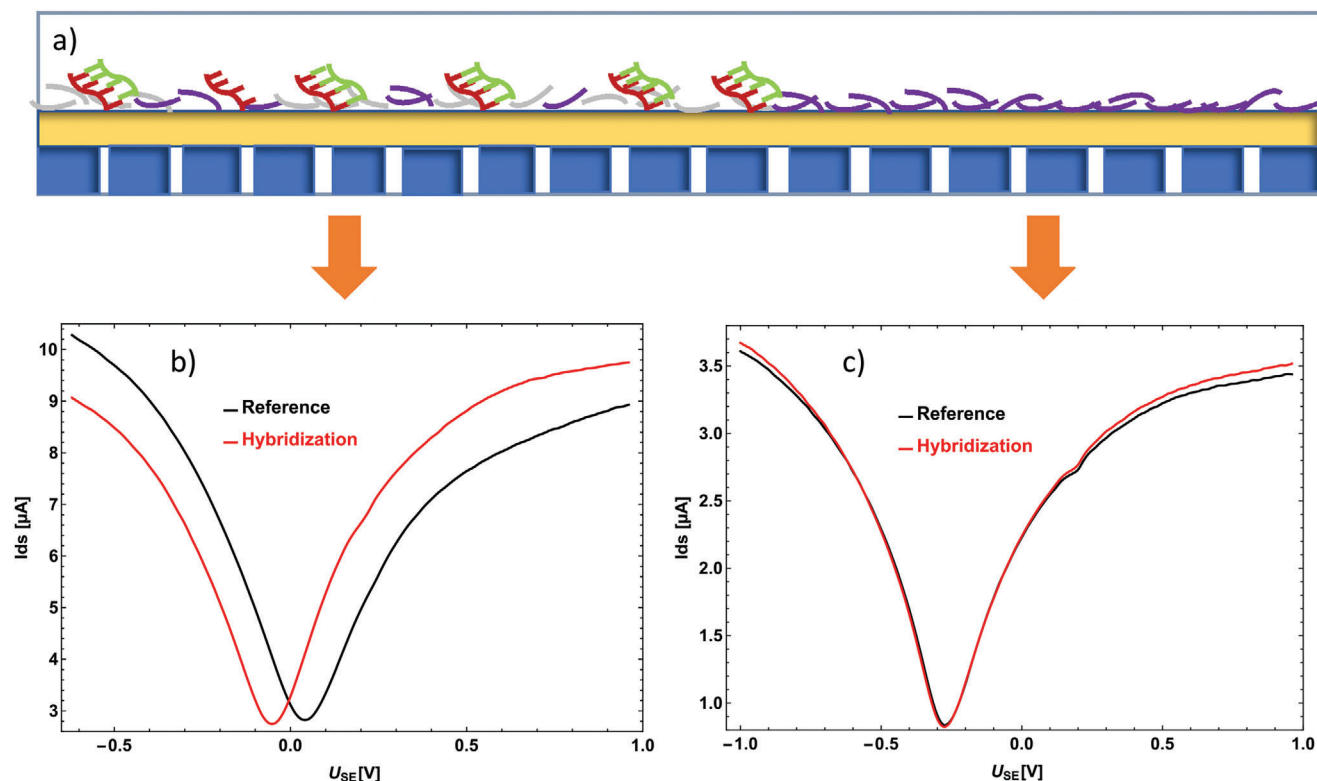


Figure 3. a) Schematic representation of the GFET array/electrolyte interface. The GFETs (blue) are covered by a thin $\text{Al}_2\text{O}_3/\text{SiO}_x$ protection layer (yellow). The latter is covered by PLL polymer, to which probe DNA (red) is electrostatically bound (active PLL gray and neutralized PLL violet). b) Specific hybridization of negatively charged target DNA (green in panel [a]) induces a left shift of the Dirac point. c) GFETs without probe DNA were used as a control where no binding occurs. No shift occurred for these reference GFETs, $U_{\text{DS}} = 10$ mV.

via the PLL layer. The surface is covered by an aqueous solution and hybridization occurs between the target molecules in the solution and the surface-attached probes. As DNA is negatively charged in aqueous solution, the charge-density of the GFET surface decreases as a result of hybridization. A schematic view of a GFET with the functional parts for hybridization measurement is presented in Supporting Information.

DNA-hybridization is measured either by real-time monitoring of the FET current–voltage characteristics during the hybridization, or by comparing FET characteristics measured immediately before and after the hybridization period of about 20–30 min. We paid special attention to electrolyte concentrations used in measuring a charge density change at the gate insulator surface. Indeed, the change in potential induced by adsorption of charged species depends on salt concentration. The Debye screening length at the gate insulator/electrolyte interface is optimized to achieve sensitive detection of charge.

2.4. End-Point Detection of DNA Hybridization

For end-point detection of DNA hybridization we used two different aqueous solutions: one for electronic measurement and another one for hybridization. This way, sensitivity (favored by a low salt concentration during the electronic measurement) and specificity (favored by a higher salt concentration during

the hybridization) can be optimized independently.^[31] We used a 25 mM KCl solution during FET readout and a PBS solution during hybridization. For hybridization, the chip was soaked in PBS containing 10 nM of target DNA for 30 min at room temperature. Afterward, we rinsed the chip with 25 mM KCl solution to remove non-hybridized and weakly bound targets and performed electronic measurement.

In **Figure 3b** one can observe a negative shift of the Dirac point of -50 ± 23 mV after hybridization with five GFETs, where probe DNA is bound. On the other hand, no shift occurred for the reference GFETs **Figure 3c**.

To assess the specificity of the assay, three different DNA probes were deposited at different positions on the array: ARS3, ARS5, and ARS7 (**Figure 4a**). After deposition, the chip was dried and treated as previously in acetic anhydride and Lprime to avoid non-specific adsorption of target DNA. The reference measurement is shown in black. After incorporation of target (20 nM) ARS5sens, complementary to ARS5, a second measurement was performed (blue). The chip was rinsed and soaked in solution containing 20 nM of ARS3sens, complementary to ARS3 and subsequently the third electronic measurement was performed (red).

For FETs covered by ARS5, we observed a significant negative shift of the Dirac point when the chip was incubated in ARS5sens solution (-46 ± 29 mV for the 6 FETs), and only a tiny shift following incubation in ARS3sens. FETs by the ARS3 probe did not shift under ARS5sens incubation, but did for ARS3sens (-37.5 ± 29 mV for the 5 FETs). FETs by ARS7 probe did not

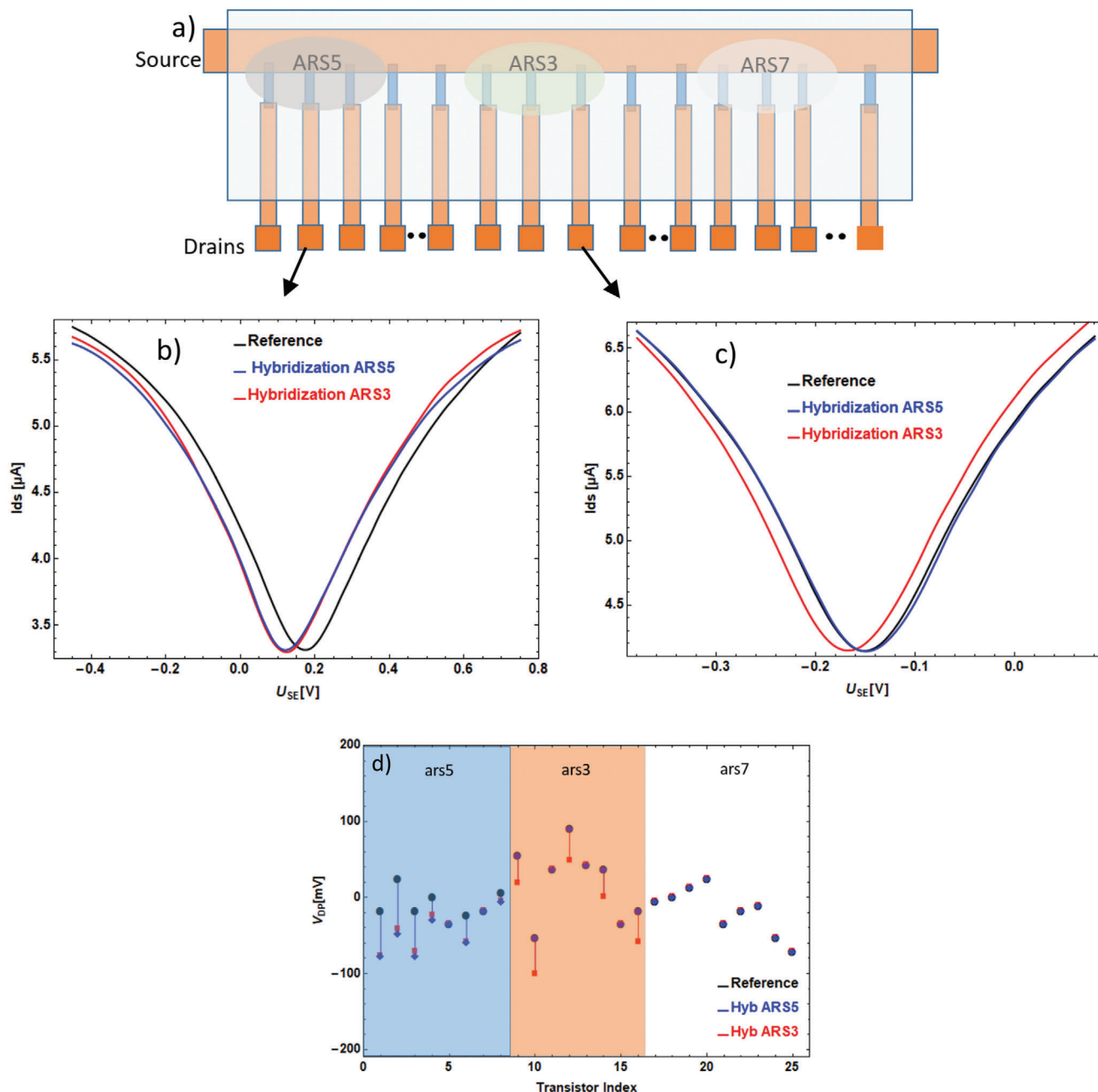


Figure 4. a) Schematic illustration of a GFET array covered by three solutions containing three different probe sequences. b) Characteristics of a FET covered by the drop of sequence ARS5. We observe a left shift of the Dirac point when the chip was soaked in ARS5sens solution and only very small shift after ARS3 hybridization. c) Characteristics of a FET covered by the drop of sequence ARS3. This transistor did not shift upon the initial ARS5 incubation but did so during the subsequent ARS3 incubation. The FETs covered by the ARS7 sequence showed no response for both incubations (image not shown). d) Panel shows the shifts of the Dirac points for the two hybridization experiments. $[KCl] = 25$ mM, $U_{DS} = 10$ mV.

respond in both incubations. This demonstrates that our device detects the different target sequences by specific hybridization. We tentatively attribute the absence of significant shifts of transistors 5, 7, 11, 13 and 15 to either a local problem of probe immobilization, or a local defect in the graphene sheet.

The experiment presented in **Figure 5** was to determine the lowest concentration of target that can be detected. Since sensitivity of the transistors decreases upon repeated usage, the

experiment was performed with a freshly prepared GFET array to have high sensitivity. The blocking steps avoid non-specific adsorption and prevent losing a significant amount of target at low concentration in this measurement. The concentration of the targets was set at 10 fM. After incubation of the chip with targets for 30 min, the chip was rinsed then three detection measurements performed every two minutes. The observed signal amplitude (−50 mV, downward-shift from −120 to −170 mV)

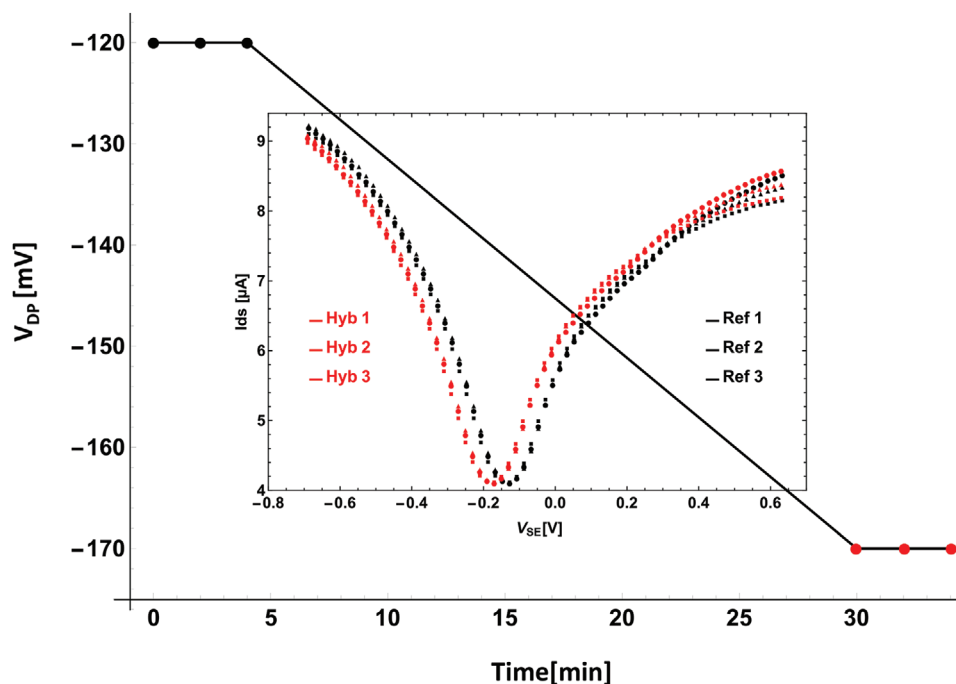


Figure 5. Device sensitivity upon 10 fM target concentration. Three reference measurements (black) triangle, square, and circle in time step of two minutes were performed after the surface blocking steps. The red curves refer to hybridization detection measurement after soaking the chip in solution containing complementary target for 30 min. [KCl] = 10 mM, $U_{DS} = 10$ mV.

strongly exceeded the experimental drift (drift is undetected on the time-scale, as illustrated by three data points before and three data points after the hybridization). This suggests it might be possible to achieve detection below the femtomolar range. One neighboring GFET was measured in parallel and also detected specific hybridization, albeit with a shift of smaller magnitude (−21 mV). We repeated the experiment with another freshly prepared GFET array. In this case, four transistors were recorded and all detected the hybridization at a 10 fM target concentration (−19, −18, −25, −22 mV). Using another freshly prepared array, we then attempted detection of hybridization at a tenfold reduced target concentration (1 fM). We measured five transistors of the array and observed a very small hybridization signal for two of them (shifts of about −5 and −6 mV), but otherwise did not observe a shift that clearly exceeded the measurement uncertainty of about 2 mV. For the measurements presented herein, the measurement uncertainty is mainly given by the precision of the Dirac point voltage determination, which depends on the step-size of the discrete U_{SE} voltage recordings (here 10 mV), and the width of the I_{DS} minimum (depending on charge-carrier mobility, see Discussion section).

2.5. Real-Time Measurement of DNA Hybridization

Real-time or in situ measurement of DNA hybridization is more challenging than end-point detection, because it requires using the same salt concentration for both hybridization and electronic measurement. It is worth the effort, since it provides access to the kinetics of the hybridization that contains valuable informa-

tion. One application is the dynamic allele-specific hybridization (DASH) assay^[32] for scoring single nucleotide polymorphism (SNP).

For the measurements presented in **Figure 6**, we immobilized ARS3 probe oligonucleotides on PLL, dried for 45 min and subsequently used chemical and physical blocking, as described before. A (0.1× PBS) solution containing ARS3sens target at 40 nM was used as electrolyte and hybridization solution. A series of ten measurements every 3 min was performed (Figure 6a). Immediately afterward, the hybridization solution was replaced by a 0.1× PBS solution containing ARS5sens (at 40 nM) and a second series of ten measurements performed. Figure 6 shows the transfer curves (panels [a] and [b]) and the Dirac point locations (panel [c]) during these measurements. We observed a progressive negative shift of the Dirac point during the first 16 min. The duration of the shift was 20 ± 5 min for 7 FETs (obtained from three different chips) measured under the same conditions. At the beginning the shift increases rapidly, with an initial Dirac point displacement of about 2.8 mV min^{-1} . The rate of change progressively decreases toward zero. Such shifts never appeared during measurements with non-complementary target.

3. Discussion

Although in our case detection occurred in the presence of an insulating layer on top of the GFET array, we have been able to detect hybridization of target DNA molecules down to femtomolar concentrations (Figure 5). Our devices are stable in contact with aqueous solutions (Figure S2, Supporting Information) and exhibit only very weak threshold voltage drifts. Chen et al.^[29] and

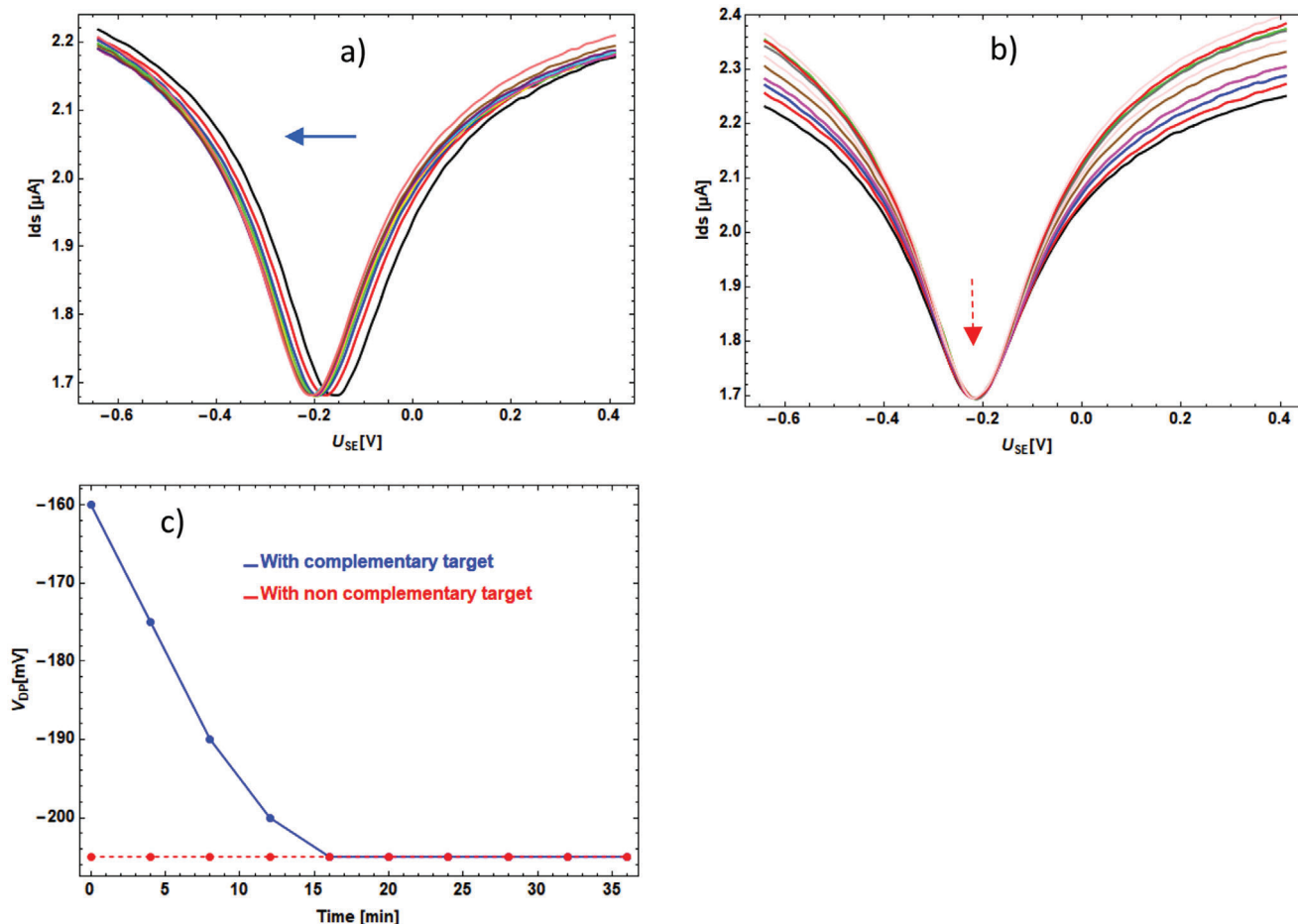


Figure 6. a) Series of current–voltage characteristics measured during hybridization with the complementary target (ARS3sens). b) Series of characteristics measured during subsequent incubation with a non-complementary target (ARS5sens). c) Dirac point locations during the two measurements as a function of time. The Dirac point shifted by about 50 mV during the initial 16 min of the specific hybridization and then stabilized. It never shifted during measurements with non-complementary target, $U_{DS} = 10$ mV.

Dong et al.^[17] performed measurements under conditions of hybridization that were similar to ours, but fixed the DNA probe molecules by adsorption directly onto the graphene sheet. The sensitivity of their devices was estimated to be in the picomolar range. Rui et al.^[20] also worked without an insulating layer and used a crosslinking agent (1-pyrenebutyric acid succinimidyl ester, PBSE) to attach amine-modified DNA to the graphene. A positive shift was obtained upon DNA hybridization and attomolar sensitivity achieved. They attributed the high sensitivity to the fact that their transistor channel is at the center of a surrounding two-lobed annular gate, which provided a uniform distribution of electric potential in the vicinity of the channel. Xu et al. used the biotin-streptavidin system for attachment of DNA probes to graphene FETs and reported DNA hybridization detection with a sensitivity of 100 fM–1 pM.^[30]

We achieved reproducible detection of hybridization with 20 mer DNA oligonucleotides at 10 fM concentration. Hybridization of a single target molecule corresponds to formation of 20 DNA base pairs. The detection limit of 10 fM of target molecules thus corresponds to a 200 fM detection limit in terms of individual DNA base pairs. We attribute the high sensitivity to good trans-

ducing capability of GFET arrays made possible by two original elements. First, shifts of the Dirac point due to incorporation of impurities during device fabrication is detrimental to sensitivity. We reduced such shift by an innovative fabrication process that protects the graphene during photolithographic patterning (see Experimental Section). The as-fabricated GFETs exhibited high mobility and the Dirac point location is well defined, as shown by the steep V-shape like current–voltage characteristics. Indeed, small threshold-voltage shifts induced by DNA hybridization are more easily resolved if the Dirac point manifests itself as a sharp peak. Second, we used a thin protection layer that separates the graphene from the electrolyte solution during DNA hybridization and electronic measurement. The composition and thickness of this dielectric layer was optimized to achieve both sensitivity and stability of threshold voltage under electrolyte (i.e., very small residual drift). We found a good solution to this non-trivial optimization, a double-layer deposited by ALD and PECVD, as described in Experimental Section.

Our devices exhibit a surface configuration similar to silicon-based electrolyte-gated FETs, as the graphene channels are covered by a thin insulator layer. This layer provides time

stability to the device characteristics and avoids chemical contamination of graphene during contact with electrolyte solutions. The surface in contact with the electrolyte is SiO₂, as for the silicon arrays used in previous electronic measurements of DNA hybridization.^[3,4,31] Moreover, the salt compositions of the electrolyte solutions used herein are similar to studies with silicon arrays. As expected, the signs of the threshold voltage shifts observed (upon PLL adsorption, DNA adsorption, and DNA hybridization) coincide with the ones described for silicon devices. Remarkably, our GFET devices exhibit very small threshold-voltage drifts (below 1 mV per hour, see Figures 2b, 5, and 6), much smaller than the ones observed with silicon devices (about 0.2–1 mV min⁻¹, see for instance, refs. [4,33,34]). In addition, the amplitudes of the electronic signals of DNA hybridization are about 100 mV for our GFET arrays, strongly exceeding the typical 3–10 mV amplitudes of silicon FET arrays (see refs. [3,4,31]). The combination of small drift and high signal amplitude greatly facilitates real-time DNA hybridization detection when compared to silicon devices, as illustrated in Figure 6.

The exposed surface of our protection layer is composed of SiO_x, which from a surface chemistry point of view is similar to the glass (SiO₂) surface used in standard DNA microarrays with fluorescence detection. Therefore, the various strategies for surface-functionalization used in the microarray field could also be used with our GFET arrays. The procedure of probe immobilization, blocking of non-specific DNA adsorption, and salt conditions of hybridization used in the present work allow for base sequence recognition with high specificity. Specificity is shown in Figure 4, where three different 20mer base sequences were used in parallel. Longer probe sequences could be employed, but the choice of short oligonucleotide probes (12–25 mer) favors specificity, and single base pair specificity has been reported in the literature.^[4] Of note, single-stranded probe molecules are preferred to double-stranded ones to assure that base sequences are readily accessible to hybridization, but chemical synthesis of single-stranded DNA becomes increasingly difficult for lengths beyond 100 nucleotides.

In this work, we used standard 20 mer DNA oligonucleotides as target DNA for label-free detection of DNA hybridization by GFET arrays. If the electronic detection would be integrated in a biological assay, target DNA or RNA molecules could be detected following synthesis by an enzymatic amplification like PCR. For instance, we have previously described DNA genotyping by a multiplex assay combining tagged allele-specific polymerase chain reaction (Tas-PCR) and field-effect transistor-based hybridization.^[3]

In the perspective of future work, it would be desirable to increase the charge carrier mobility of the GFET array, to improve the stability of the sensors upon repeated usage and to reduce the variations in their specifications (within a GFET array as well as from one array to another). Possible routes include the use of sapphire^[35] or hexagonal boron-nitride^[36] substrates, which provide higher mobility even at room temperature.

4. Conclusions

GFET arrays based on transferred CVD-grown graphene were developed for label-free detection of DNA hybridization. Single-

Table 1. Dirac point voltages under ambient conditions (Figure 1).

	V _{DP} [V]	Sample size
Sample 1	4 ± 17	43
Sample 2	19 ± 10	46
Sample 3	20 ± 15	48

stranded DNA was immobilized onto the surface of a PLL coated chip. Adsorption of positively charged PLL polymer induced a right shift of the Dirac point, whereas adsorption of negatively charged DNA probes triggered a left shift. Differential and real time in situ measurements of DNA hybridization were performed. This demonstrated that GFET arrays can detect target DNA molecules down to femtomolar levels, even though detection is achieved through an insulating layer. Our devices exhibited very stable threshold-voltages and the combination of high sensitivity and low drift allowed for real time hybridization detection. Thus, passivated GFET arrays have great potential, particularly for applications where graphene sheet integrity is needed and the quantity of target DNA to be detected is low.

5. Experimental Section

Fabrication of the GFET Arrays: The GFET arrays were fabricated using conventional photolithography on pieces of 12 mm × 12 mm of a thermally oxidized p-doped Si wafer. The high-quality thermally grown SiO₂ (thickness 1 μm) served as gate insulator for back gate measurements. The wafer pieces were cleaned ultrasonically in acetone and isopropanol, 5 min each, dried with nitrogen and treated in plasma cleaner chamber to make them more hydrophilic. Commercial CVD-grown graphene (Graphenea, San Sebastián, Spain) was transferred from its copper substrate onto the Si wafer pieces and dried for 45 min to enhance the adherence of graphene sheet to substrate and soaked in hot acetone (50 °C) for more than 15 min to remove the PMMA used to protect the graphene sheet during the transfer. A thin Al₂O₃ layer (1 nm) was deposited by ALD to protect the graphene from the photoresist and developer during subsequent photolithography. Photoresist AZ5214E was spin-coated (30 s, 4000 rpm) and baked at 110 °C for 2 min. UV exposure (≈10 mW cm⁻², 15 s) was performed using an MJB4 mask aligner, followed by AZ726MIF development for 22 s. The graphene was patterned into 48 individual channels using an optical mask. The protecting layer was etched by orthophosphoric acid (50 °C, 3 min) followed by rinsing in DI water for 2 min and the undesired graphene removed by RIE (Reactive Ion Etching, 2 min). Usually this photoresist was removed in hot acetone. But this often led to unwanted damage or loss of the alumina protecting layer owing to the hydrophobic nature of graphene. To avoid this problem, the channel resist was intentionally conserved and an additional photoresist layer (AZ5214E) was spin-coated for definition of the contacts. This procedure was possible because AZ5214E was a reversible photoresist. The resist was baked (110 °C, 2 min), exposed (2 s) through the appropriate mask, reverse-baked (125 °C, 2 min), and flood-exposed (15 s). This way, the graphene channel was protected from non-intentional doping by a double protection layer, consisting of Al₂O₃ and the photoresist. The sample was overdeveloped for 1 min to etch the protecting layer on the contact area. Titanium (10 nm) and gold (180 nm) were deposited by thermal evaporation. After removing the photoresist layers and unwanted metal residues by soaking in acetone for 15 min at 50 °C, passivation layers of 40 nm Al₂O₃ and 50 nm SiO_x were deposited by ALD at 175 °C and PECVD at 280 °C, respectively. The passivation layers were patterned on the Ti/Au electrodes. The fabricated GFET array was mounted on a commercial ceramic chip carrier and wire-bonded. Finally, a plastic well was attached to protect the wiring during subsequent liquid incubations.

Table 2. PLL adsorption (Figure 2).

Sample 1															
N°FET	1	4	5	7	8	9	18	32	36	40	41	42	43	47	Mean ± SD
PLLshift [mV], C ₀	20	80	20	140	240	240	240	200	40	240	280	320	280	300	185 ± 104
Sample 2															
N°FET	2	7	8	9	10	20	22	27	30	32	42	44	45	46	Mean ± SD
PLL [mV] C ₀ /2	64	62	90	48	66	96	56	84	90	96	50	60	68	80	72 ± 17

Table 3. DNA hybridization (Figure 3).

Sample 1															
N°FET	2	4	5	7	8	9	18	36	39	41	42	47		Mean ± SD	
Hyb [mV]	0	0	0	-20	-60	-70	0	0	-80	-60	0	0		-50 ± 23	
Sample 2															
N°FET	1	3	5	7	9	11	17	37	39	41	47		Mean ± SD		
Hyb [mV]	0	0	0	0	0	0	-30	-80	-100	-80	-20		-62 ± 35		
Sample 3															
N°FET	24		26		30		34		42		44		48	Mean ± SD	
Hyb[mV]	-20		-30		-60		-20		0		0		0	-32.5 ± 19	

Table 4. Specificity of DNA hybridization (Figure 4).

	ΔV_{DP} [mV]	Sample size
ARSSsens	-46 ± 29	6
ARS3sens	-37.5 ± 29	5

Table 5. Real-time measurement of DNA hybridization (Figure 6).

	FET1	FET2	FET3	FET4	FET5	FET6	FET7	Mean ± SD
Time [min]	15	28	21	24	16	18	18	20 ± 5
ΔV_{DP} [mV]	-220	-180	-240	-280	-45	-160	-120	-178 ± 79

Thermal Annealing Treatment of the GFETs: If the graphene was not well protected, the graphene transfer technique and photolithography process usually induced a high p-doping of the fabricated GFETs. If such non-intentional doping of the GFETs was observed, the sample was annealed under high-vacuum (5×10^{-6} mbar) at 280 °C for 24 h. The chip was stored under vacuum. It was observed that the annealing reduced the p-doping, brought the Dirac point closer to zero-voltage, and improved the mobility. Time stability studies showed that the device characteristics (voltage and

Table 6. Thermal annealing treatment of the GFETs (Figure 7).

	As-fabricated	Post-annealing	Sample size
Sample 1 V_{DP} [V]	106 ± 38	32 ± 20	47
Sample 2 V_{DP} [V]	147 ± 31	23 ± 30	46
Sample 3 V_{DP} [V]	41 ± 17	16 ± 12	31

resistance at the Dirac point and contact resistance) were stable for more than a month after this annealing.

The drain current I_{DS} of each FET was measured as a function of both source-drain voltage U_{DS} and a voltage U_{SE} applied between a common source contact and an Ag/AgCl reference electrode immersed in KCl solution covering the array. Detailed descriptions of the experimental setup and the measurement procedures were provided in earlier publications of the authors' group.^[31,37]

Poly-Lysine Adsorption and DNA Probes Immobilization: After thoroughly rinsing the device with deionized water, the as-fabricated chip was immersed in PLL, a positively charged polymer (dilution P8920 Sigma, 0.1% wt per vol in 0.13× PBS, pH 7.2, C₀ = 85 μM monomer concentration) for 30 min, dried with air, and conserved overnight at room temperature. It was observed that the PLL adsorption induced positive shifts of the graphene Dirac point and these shifts were proportional to PLL concentration. The PLL adsorption induced positive shifts of the Dirac point, $\Delta V_{cnp} = +185 \pm 104$ mV for 15 FETs.

The 20-base oligonucleotide probes (1 μM) were immobilized, thanks to PLL adsorbed at the gate surface. Oligonucleotide probes were dissolved in phosphate buffer saline (PBS, NaCl 138 mM, KCl 2.7 mM, pH 7.4 at 25 °C). A drop of 0.1 μL of this solution covering 8 to 10 FETs was deposited on the array and dried for 45 min to withstand the next step. The probes fixation induced left shift of V_{cnp} meaning that the intrinsic negative charges of DNA made the graphene less p-doped (Figure 2d). This result agreed with the right shift observed for PLL adsorption (Figure 1c). Immobilization of the DNA probes did not fully compensate the positive charge of the PLL layer and the remaining positive charge could induce non-specific adsorption of DNA targets during the hybridization process. Therefore, efficient blocking was required for DNA detection in microarray format. A combined chemical and physical blocking procedure was performed. The non-fixed sites of PLL coating were neutralized by incubating the chip in acetic anhydride for 30 min followed by rinsing in DI water. Residual adsorption of the PLL layer was then reduced by incubating the surface with a solution containing 21-base oligonucleotides (Lprime) whose sequence was different from the complementary targets of the immobilized probes.

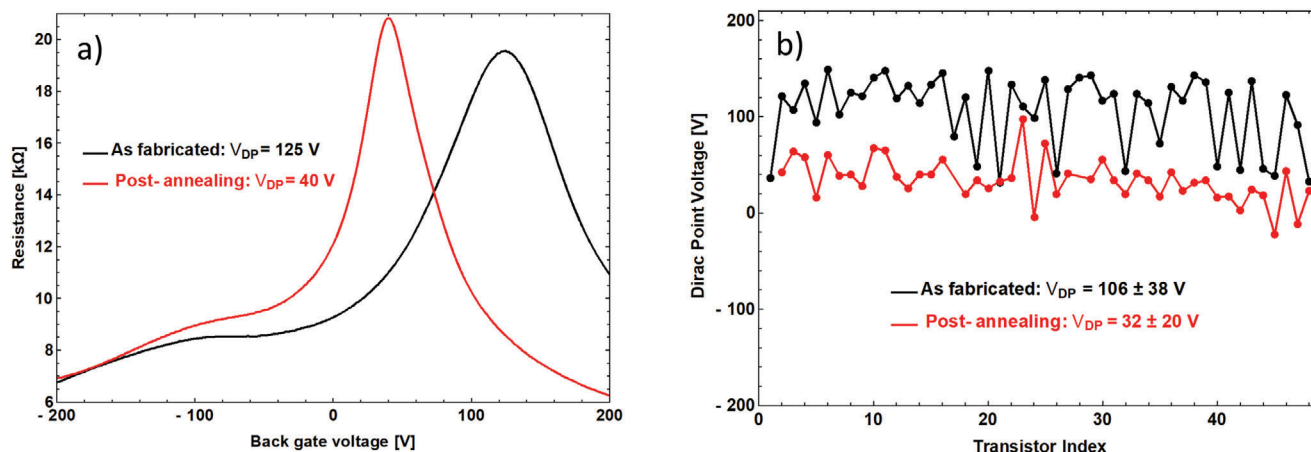


Figure 7. a) Current transfer curves of an individual FET showing the shift of the Dirac point towards zero back gate voltage after annealing. b) Dirac point locations before (black) and after (red) annealing of an FET array, $U_{DS} = 0.2$ V.

Surface densities of oligonucleotide probes immobilized by PLL on silica have been published. In an earlier study of a DNA hybridization with silicon FET arrays, PLL immobilization and local deposition were used under conditions similar to this work and probe surface densities of 10^4 – 10^5 molecules per μm^2 were evaluated.^[31] Under saturating conditions, for instance, after 16 min in Figure 6c, the surface density of hybridized targets approached the probe surface density. Fritz et al. published a similar value (3×10^4 molecules per μm^2) for the surface densities of probes and targets.^[4]

Oligonucleotide Sequences:

ARS3: 5'-CCG CGA ACT GAC TCT CCG CC-3'
 ARS5: 5'-CAG GCG GCA GGG CTG ACG TT-3'
 ARS7: 5'-TAT AGC GTA CGA ACT CCA GC-3'
 Lprime: 5'-GGG TTT TGC TAT CAC GTT GTG-3'

The sequences of the target DNA oligonucleotides ARS3sens, ARS5sens, and ARS7sens were complementary to ARS3, ARS5, and ARS7, respectively. ARS3sens and ARS7sens were Cy3-labeled at the 5' end, while ARS5sens was Cy5-labeled at the 5' end.

Statistical Analysis: This subsection contains information about the statistics behind the results presented in the article. It covers the different measurements in the order of the figures. Where appropriate, data is presented in the format mean \pm SD, and the sample size is provided (mean stands for arithmetic average and SD for standard deviation).

Table 1 shows data related to Figure 1b. The position of the Dirac point voltage of three as-fabricated chips is given for back-gated electrical measurements in ambient conditions. Sample 1 is prepared by our innovative fabrication process with graphene protection during photolithographic patterning, while samples 2 and 3 were obtained by a corresponding process without graphene protection. 43, 46, and 48 transistors of the GFET array were measured, respectively.

Table 2 shows data related to Figure 2c. Sample 1 and Sample 2 are two different GFET arrays, prepared with graphene protection. Shifts of the Dirac points under PLL adsorption are presented for 14 individual GFETs. The last column provides average and standard deviation of the two statistical ensembles. PLL concentrations were C_0 and $C_0/2$ for sample 1 and 2, respectively.

Table 3 shows Dirac point shifts during electrical DNA hybridization detection. FETs 18 and 36 of sample 1 are insensitive upon DNA hybridization. The other GFETs without shift were not covered by probe DNA and served as internal control. GFETs without shift are not included in the statistical mean \pm SD.

Table 4 provides mean, SD, and sample size of the data presented in Figure 4c.

Table 5 shows Dirac point shifting upon real-time DNA hybridization. FET (1, 2), (3, 4) and (5, 6, 7) are from three different chips, respectively.

Table 6 shows Dirac point position for as-fabricated and post-annealing treatment. The three chips were fabricated without our graphene protection during lithography.

Supporting Information

Supporting Information is available from the Wiley Online Library or from the author.

Acknowledgements

This work was financially supported by PSL Research University in the frame of the GrapheneDNA project providing a Ph.D. grant to K.M. Moreover, the authors benefitted from funding by the European Union Horizon 2020 research and innovation program (Grant No. 785219 "Graphene Core 2"). The authors thank C. Dodray for technical assistance in developing the annealing oven.

Conflict of Interest

The authors declare no conflict of interest.

Keywords

DNA hybridization, electronic detection, graphene, real-time hybridization measurement, transistor arrays

Received: February 17, 2020

Revised: June 4, 2020

Published online:

- [1] W. Wu, C. Pana, Y. Zhang, X. Wen, *Nano Today* **2013**, *8*, 619.
- [2] X. Cheng, Y. Noh, J. Wang, M. Tello, J. Frisch, R. Blum, A. Vollmer, J. Rabe, N. Koch, H. Sirringhaus, *Adv. Funct. Mater.* **2009**, *19*, 2407.
- [3] A. Blin, I. Cissé, U. Bockelmann, *Sci. Rep.* **2014**, *4*, 4194.

- [4] J. Fritz, C. Emily, G. Suzanne, S. Peter, M. Scott, *Proc. Natl. Acad. Sci. U. S. A.* **2002**, *99*, 14142.
- [5] P. Fromherz, A. Offenhausser, T. Vetter, J. Weis, *Science* **1991**, *252*, 1290.
- [6] Z. Gao, A. Agarwal, A. Trigg, N. Singh, C. Fang, C.-H. Tung, Y. Fan, K. Buddharaju, J. Kong, *Anal. Chem.* **2007**, *79*, 3291.
- [7] G. He, J. Li, H. Ci, C. Qi, X. Guo, *Angew. Chem., Int. Ed.* **2016**, *55*, 9036.
- [8] J. Veerbeek, R. Steen, W. Vijeelaar, F. Rurup, S. Korom, A. Rozzi, R. Corradini, L. Segerink, J. Huskens, *Langmuir* **2018**, *34*, 11395.
- [9] G. Jayakumar, M. Legallais, P.-E. Hellström, M. Mouis, I. Pignot-Paintrand, V. Stambouli, C. Ternon, M. Östling, *Nanotechnology* **2019**, *30*, 0957.
- [10] M. Nuzaihan, U. Hashim, M. Arshad, R. Ruslinda, A. Rahman, M. Fathil, M. Ismail, *PLoS One* **2016**, *11*, 0152318.
- [11] J. Kim, S.-Y. Park, S. Kim, D. H. Lee, J. H. Kim, J. M. Kim, H. Kang, J.-S. Han, J. W. Park, H. Lee, S.-H. Choi, *Sci. Rep.* **2016**, *6*, 31984.
- [12] E.-L. Gui, L.-J. Li, P. Lee, A. Lohani, S. Mhaisalkar, Q. Cao, S. Jun, J. Rogers, N. Tansil, Z. Gao, *Appl. Phys. Lett.* **2006**, *89*, 232104.
- [13] A. Star, E. Tu, J. Niemann, J.-C. Gabriel, S. Joiner, C. Valcke, *Proc. Natl. Acad. Sci. U. S. A.* **2005**, *103*, 921.
- [14] N. Green, M. Norton, *Anal. Chim. Acta* **2014**, *853*, 127.
- [15] L. Hess, M. Seifert, J. Garrido, *Proc. IEEE* **2013**, *101*, 1780.
- [16] X.-m. Chen, G.-h. Wu, Y.-q. Jiang, Y.-r. Wang, X. Chen, *Analyst* **2011**, *136*, 4631.
- [17] X. Dong, Y. Shi, W. Huang, P. Chen, L. Li, *Adv. Mater.* **2010**, *22*, 1649.
- [18] B. Cai, S. Wang, L. Huang, Y. Ning, Z. Zhang, G.-J. Zhang, *ACS Nano* **2014**, *8*, 2632.
- [19] N. Mohanty, V. Berry, *Nano. Lett.* **2008**, *8*, 4469.
- [20] R. Campos, J. Borme, J. R. Guerreiro, G. Machado, *ACS Sens.* **2019**, *4*, 286.
- [21] A. Mart, S. Jockusch, N. Stevens, J. Ju, N. Turro, *Acc. Chem. Res.* **2007**, *40*, 402.
- [22] L. Smith, J. Sanders, R. Kaiser, P. Hughes, C. Dodd, C. Connell, C. Heiner, S. Kent, L. Hood, *Nature* **1986**, *321*, 674.
- [23] N. Tansil, Z. Ga, *Nano Today* **2006**, *1*, 28.
- [24] M. Pardue, J. Gall, *Proc. Natl. Acad. Sci. U. S. A.* **1969**, *64*, 600.
- [25] C. Zhao, L. Wu, J. Ren, X. Qu, *Chem. Commun.* **2011**, *47*, 5461.
- [26] M. Abbott, B. Poiesz, B. Byrne, S. Kwok, J. Sninsky, G. Ehrlich, *J. Infect. Dis.* **1988**, *158*, 1158.
- [27] K. Yeon, D. Choi, Y. Kim, H. Kima, D. Yoon, S.-S. Ahn, J.-W. Yang, W. Yang, S. Seo, *Biosens. Bioelectron.* **2012**, *37*, 82.
- [28] D. Khatayevich, T. Page, C. Gresswell, Y. Hayamizu, W. Grady, M. Sarikaya, *Small* **2014**, *10*, 1505.
- [29] T.-Y. Chen, P. T. K. Loan, C.-L. Hsu, Y.-H. Lee, J. T.-W. Wang, K.-H. Wei, C.-T. Lin, L.-J. Li, *Biosens. Bioelectron.* **2013**, *41*, 103.
- [30] G. Xu, J. Abbott, L. Qin, K. Yeung, Y. Song, H. Yoon, J. Kong, D. Ham, *Nat. Commun.* **2014**, *5*, 4866.
- [31] C. Gentil, G. Philippin, U. Bockelmann, *Phys. Rev. E* **2007**, *75*, 011926.
- [32] M. Howell, M. Jobs, U. Gyllensten, A. Brookes, *Nat. Biotechnol.* **1999**, *17*, 87.
- [33] K. Malpartida-Cardenas, N. Miscourides, J. Rodriguez-Manzano, *Biosens. Bioelectron.* **2019**, *11*, 0956.
- [34] C. Perréard, A. Blin, U. Bockelmann, *Sens. Actuators, B* **2013**, *282*.
- [35] E. Pallecchi, C. Benz, A. Betz, H. Löhneysen, B. Plaçais, R. Danneau, *Appl. Phys. Lett.* **2011**, *99*, 113502.
- [36] W. Yang, S. Berthou, X. Lu, Q. Wilmar, A. Denis, M. Rosticher, T. Taniguchi, K. Watanabe, G. Fève, J. Berroir, G. Zhang, C. Voisin, E. Baudin, B. Plaçais, *Nat. Nanotechnol.* **2018**, *13*, 47.
- [37] F. Pouthas, C. Gentil, D. Côte, G. Zeck, B. Straub, U. Bockelmann, *Phys. Rev. E* **2004**, *70*, 031906.